

Article

Numerical Equivalent Acoustic Material for Air-Filled Porous Absorption Simulations in Finite Different Time Domain Methods: Design and Comparison

P. C. Iglesias ^{1,*} , L. Godinho ²  and J. Redondo ¹ 

¹ Instituto de Investigación para la Gestión Integrada de Zonas Costeras, Universitat Politècnica de València, Campus de Gandía, C. Paranimf, 1, 46730 Gandia, Spain; fredondo@fis.upv.es

² Departamento de Engenharia Civil, Universidade de Coimbra, ISISE, ARISE, R. Luis Reis dos Santos 290, 3030-790 Coimbra, Portugal; lgodinho@dec.uc.pt

* Correspondence: pabcamig@gmail.com

Abstract: Extracting the microscopic parameters of a porous material is a complex task, and attempts have been made to develop models that can simulate their characteristics, gathering the least amount of information possible. As a case in point, tests to evaluate macroscopic behaviors such as tortuosity, which depends directly on the microscopic fluid velocities, are highly susceptible to generate errors if the precision of the measurement devices is not correct, and the same goes for the other parameters. For this reason, in this paper, a sound propagation model in porous materials with a rigid frame is presented based on a local theory, which tries to simplify, even more, the way to obtain the basic characteristics of porous materials, such as their absorption coefficient at normal and random incidence, and their normal surface impedance. The proposed linearized equivalent fluid model presents four phenomenological coefficients, which characterize acoustic propagation through the material. Their values are obtained from the material thickness and a measurement in an impedance tube following the ISO 10534 standard. Thus, what is only required is the measured absorption coefficient, either on one third or one octave bands, to fully represent the acoustic behavior in the finite different in time domain (FDTD) method. The model has been simulated with FDTD in porous and fibrous kernels, and the results show a strong agreement with the laboratory measurements and with the analytical results calculated with well-established semi-phenomenological models.

Keywords: porous absorber; FDTD; equivalent porous material



Citation: Iglesias, P.C.; Godinho, L.; Redondo, J. Numerical Equivalent Acoustic Material for Air-Filled Porous Absorption Simulations in Finite Different Time Domain Methods: Design and Comparison. *Appl. Sci.* **2024**, *14*, 1222. <https://doi.org/10.3390/app14031222>

Academic Editor: Kimihiro Sakagami

Received: 15 December 2023

Revised: 23 January 2024

Accepted: 30 January 2024

Published: 1 February 2024



Copyright: © 2024 by the authors. Licensee MDPI, Basel, Switzerland. This article is an open access article distributed under the terms and conditions of the Creative Commons Attribution (CC BY) license (<https://creativecommons.org/licenses/by/4.0/>).

1. Introduction

Frequently, sound propagation inside the pores of porous absorbers is described by its effective density, without thermal effects, and an effective bulk modulus, without viscous effects [1]. As waves can propagate through the material pores, it is reasonable to consider that some energy is transmitted to the frame. In that case, no rigid frame is considered. Instead, an elastic frame should be used. Biot et al. [2,3], conceive a model in which this behavior is presented as a set of tensors for strains and displacements.

Years later, an empirical method was developed by Delany and Bazley [4], in which the absorption process is taken into account by means of the material characteristic impedance and its wavenumber, both being complex numbers. A large number of impedance tube measurements were performed, and afterwards, absorption coefficients were fitted into a power law relation. As a result, a set of equations are given and, from them, it is possible to calculate porous absorption in a wide frequency range.

Considering that the solid skeleton can often be set as immobile, and non-deformable, the acoustic movements are those of the saturating fluid, normally air, affected by viscous friction and thermal exchanges at the pore walls [5]. In harmonic regime, the material

can be described, at macroscopic level, as an equivalent fluid, by following local equations [6]. In local theory, where a surface point is described by itself, without neighboring point's dependence, the material is characterized by the effective density and the effective compressibility, which are, respectively, $\rho_f \alpha(\omega)$ and $\beta(\omega)/K_a$ [5,7],

$$\rho_f \alpha(\omega) \frac{\partial \mathbf{u}_m}{\partial t} = -\nabla p_m \tag{1}$$

$$\frac{\beta(\omega)}{k_f} \frac{\partial p_m}{\partial t} = -\nabla \mathbf{u}_m \tag{2}$$

where ρ_f is the static fluid density, \mathbf{u}_m the material particle velocity, p_m the material pressure and k_f the static fluid compressibility. Subscript m denotes "material" in order to differentiate from fluid values.

Those terms are governed by the dynamic tortuosity, $\alpha(\omega)$, and the dynamic compressibility, $\beta(\omega)$, of the air immersed in the material pores, and are frequency dependent. Their theoretical expressions were given initially by Johnson [8], and later modified by Lafarge in the so-called JCAL (Johnson–Champoux–Allard–Lafarge) model [7], being the most used phenomenological model to calculate sound absorption in porous materials. The JCAL model uses six parameters to fully represent the porous absorber performance, being the open porosity, the static air-flow resistivity, the dynamic tortuosity, the viscous and thermal lengths and, finally, the thermal permeability. Jaouen et al. [9], clearly attempt to a direct evaluation of the six parameters through a simple impedance tube measurement. Regardless of how they extracted the data to obtain a representative value for the parameters, they showed some limitations to this method, such as leakages around the sample or the internal vibrations in the material skeleton. These drawbacks could have a high impact in the final characterization of the material. In a similar manner, Niskanen et al. [10], relied on the porous material characterization by also using a set of impedance tube measurements. An equivalent density and bulk modulus was considered by fitting the measured and modeled values to outline the JCAL parameters. Resembling the mentioned methods is the use of the six parameters given by the JCAL model to represent the acoustical performance of porous materials.

The recurrence taken in the JCAL model makes necessary to relate the absorption mechanisms, which are given by the dynamic tortuosity and the dynamic permeability in Equations (1) and (2), due to the viscous and thermal exchanges between the air and the material structure [11]. Fluid parts affected by these exchanges can be estimated by the pore size ratio to the viscous skin depth thickness, $\delta = (2\eta/\omega\rho_0)^{1/2}$, where η is the fluid shear viscosity and ω the angular frequency. The skin depth, δ , also controls the limit for low- and high-frequency approximations [11]. In addition, the limit is given when the skin depth is much bigger than the pore radius. For frequencies under the low frequency limit, viscous losses are important all over the fluid, and the generalized governing equations, in time domain, are [5],

$$\rho_f \alpha_0 \frac{\partial \mathbf{u}_m}{\partial t} + \frac{\eta\phi}{k_0} \mathbf{u}_m = -\nabla p_m \tag{3}$$

$$\frac{\gamma}{k_f} \frac{\partial p_m}{\partial t} = -\nabla \mathbf{u}_m \tag{4}$$

where α_0 is the low frequency tortuosity approximation, ϕ is the material porosity, k_0 is the static permeability, and γ is the specific heats ratio (C_p/C_v). The propagation velocity can be calculated as $c_m = (\rho_m \alpha_0 \gamma / k_f)^{1/2}$.

When frequency increases, the skin depth becomes small and the viscous effects only concentrate near the pore boundaries, and so they can be neglected [5]. For this case, the governing equations arise to the high-frequency approximation [6],

$$\rho_m \alpha_\infty \frac{\partial \mathbf{u}_m}{\partial t} + 2 \frac{\rho_m \alpha_\infty}{\Lambda} \sqrt{\frac{\eta}{\pi \rho_m}} \int_{-\infty}^t \frac{\partial \mathbf{u}_m / \partial t'}{\sqrt{t-t'}} dt' = -\nabla p_m \tag{5}$$

$$\frac{1}{K_f} \frac{\partial p}{\partial t} + 2 \frac{\gamma - 1}{K_f \Lambda'} \sqrt{\frac{\eta}{\pi Pr \rho_m}} \int_{-\infty}^t \frac{\partial p / \partial t'}{\sqrt{t-t'}} dt' = -\nabla \mathbf{u}_m \tag{6}$$

where α_∞ is the static tortuosity, Λ is the viscous characteristic length, Λ' is the thermal characteristic length and Pr is the Prandtl number.

The behavior described in Equations (5) and (6) is clearly frequency dependent and, due to the convolution term, renders it difficult to be taken into account in time domain models. Furthermore, in the literature, the number of porous material models available for application in a time domain is relatively low. Indeed, some analytical models exist for rigid frame porous materials, but their high computational-cost make them un-practical for application and implementation.

Regardless of the complexity in implementing Equations (5) and (6) in the time domain, efforts have been made to reduce the requirements of such parameters. Horoshenkov et al. [12], developed an analytical method in which the acoustical behavior of porous materials can be represented with just three parameters, being the porosity, the median pore size, and the standard deviation in the pore size. They also show that it is not necessary to use the six non-acoustical parameters given in the JCAL model to represent the performance of porous materials. For this reason, reducing the initial, unknown JCAL parameters would allow for the easiest improvement in FDTD implementations.

Most FDTD models dealing with porous materials found in the literature are based on the Zwikker and Kosten (ZK) equations [13], which, in fact, are the simplest way to have a porous absorber without excessive computational requirements. Escolano et al. [14], analyzing porous materials, make use of a variable called “aerodynamic drag parameter” (λ), which, in their model, is the only factor of air flow resistance through the material. As can be seen in the reference, this methodology involves one more equation per dimension, which generates the need for more computational resources. Wilson et al. [15], points out the use of a boundary condition for the reflections caused by a porous material, achieving frequency-dependent impedance via ZK equations using a two-parameter model. The advantage of this method is that it does not require evaluating the particle velocity and the pressure in the material. However, the two-parameter approach requires its comparison with the relaxation model [16], giving an equivalent set of ZK equations. Van Renterghem et al. [17], make use of a similar approach, also by means of ZK equations, which modifies Euler and momentum equations to

$$\rho' \frac{\partial \mathbf{u}}{\partial t} + R' \mathbf{u} = -\nabla p \tag{7}$$

$$\frac{1}{\rho' c'^2} \frac{\partial p}{\partial t} = -\nabla \mathbf{u} \tag{8}$$

where $\rho' = \rho_0 k_s / \varphi$, being k_s the structure factor, φ porosity, $c' = c_0 / \sqrt{k_s}$ and R' is the flow resistivity.

This is a straightforward approach to describe sound propagation in a porous material, and it exhibits a lower computational cost. The drawback of the model is the difficulty in finding the indicated parameters for each type of simulated material. Ferreira et al. [18], use the Rayleigh method developed by Suzuki [19], adding a “moving frame” to the constitutive equations that represents the acoustic behavior at low frequencies. At the bottom, the Rayleigh method resembles the initial ZK formulation for porous materials. However, instead of having a homogeneous layer, the material is represented as a set of

thin rigid pipes which let the air pass in between [19]. Recently, Jing Zhao et al. [20], developed a method where they manage the effective density and the effective compressibility through infinite impulse response (IIR) filters. Temporal convolutions that follow from Equations (25) and (26) in reference [5] are avoided thanks to the use of a Z-transform to the IIR function transfer. Also, to employ this method, it is mandatory to Z-transform the constitutive equations. The material's characteristic impedance is measured then, and from it, all calculations can be performed. Alomar et al. [21] describe the porous material propagation in a similar manner as the JCAL model, by using an effective density and effective compressibility, which are expressed in terms of partial fraction expansions. Such an approach forces the use of nine auxiliary functions (for 2D cases) as well as two boundary conditions that reflects the acoustic air-material interface capability.

All the FDTD methods outlined in previous paragraphs have something in common: they rely on the ZK equations to account for the drag forces on a porous material; most of them use additional constitutive, or auxiliary, equations to describe internal propagation through the material; they need multiple measurements to completely characterize the unknown parameters, highlighting that measurement protocols are very susceptible to errors due to their accuracy. In the present paper, the proposal of a Numerical Equivalent Acoustic Material (NEAM), with equivalent properties that allow an accurate simulation of material's behavior, using time domain analysis, is presented. NEAM model exchanges the effective density and the effective compressibility parameters for some phenomenological coefficients that must be adapted to achieve simulated absorption coefficient results that are equal to those measured in a Kundt tube. A similar strategy was taken into account by Dragonetti et al. [22], for the optimization of the non-acoustic parameters of a porous material, following the methods of Hamet [23], and Allard-Biot, [24]. From acoustic impedance measurements performed in a Kundt tube, and proceeding with a least squares minimization method, they were able to adjust the real and the numerical impedances and wavenumber, thus creating what the authors call an "Artificial Porous Material". In another work by the same authors [25], an analogous optimization procedure can be observed to obtain, in this case, the parameters of a fibrous material.

The paper structure is as follows. First, the materials and methods section is introduced, describing the governing equations and the numerical FDTD method for its solution, as well as the NEAM concept and the algorithm for determining its coefficients. Then, a section related to results presentation and their discussion is given, illustrating the application of the proposed strategies to different absorbing materials.

2. Materials and Methods

This section presents the tools used in this paper. In Section 2.1, the NEAM model is presented, a result of the work developed for this document. Section 2.2 introduces a strategy proposal to obtain the NEAM coefficients from impedance tube measurements. Section 2.3 briefly describes the FDTD method, being considered the core of the manuscript simulation environment. In Section 2.4, the FDTD model setup to perform the required simulations and to estimate oblique incidence or random incidence sound absorption is given. Finally, in Section 2.5, the experimental setup is presented.

2.1. NEAM Model

Inside a porous material, the sound propagation can be described, in time domain, with Equations (1) and (2). Likewise, in frequency domain, with $e^{i\omega t}$ notation, the equations convert to the following:

$$i\omega\rho_{ef}\hat{V}_m = -\nabla\hat{P}_m \quad (9)$$

$$i\omega C_{ef}\hat{P}_m = -\nabla\hat{V}_m \quad (10)$$

Being $i = \sqrt{-1}$, ρ_{ef} is the effective density $\rho_f\alpha(\omega)$, C_{ef} is the effective compressibility $\frac{\beta(\omega)}{k_f}$, and \hat{V}_m and \hat{P}_m are the frequency-dependent particle velocity and pressure, respectively.

Following the work of Alomar et al. [21], the use of partial fraction expansion in the effective density and the effective compressibility takes the form of the following:

$$\rho_{ef}(\omega) \approx \rho_{\infty} + \sum_{k=1}^{Np} \frac{A}{i\omega + a_k} \tag{11}$$

$$C_{ef}(\omega) \approx C_{\infty} + \sum_{k=1}^{Nc} \frac{B}{i\omega + b_k} \tag{12}$$

where ρ_{∞} and C_{∞} are the asymptotic values of density and compressibility when the frequency tends to infinity, A and B are real function constants, and a_k and b_k are the function poles. As stated by Moufid et al. [26], poles must be positive to get stable solutions.

Substituting (11–12) into (9–10), with the addition of the auxiliary functions φ_m and Φ_m , the inverse Fourier transform yields [27],

$$\rho_{\infty} \frac{\partial \mathbf{u}_m}{\partial t} + \sum_{k=1}^{Np} A \mathbf{u}_m - \sum_{k=1}^{Np} A a_k \varphi_m = -\nabla p_m \tag{13}$$

$$\frac{1}{\rho_{\infty} c_{\infty}^2} \frac{\partial p_m}{\partial t} + \sum_{k=1}^{Nc} B p_m - \sum_{k=1}^{Nc} B b_k \Phi_m = -\nabla \mathbf{u}_m \tag{14}$$

where $c_{\infty} = 1/\sqrt{\rho_{\infty} C_{\infty}}$ is the asymptotic sound speed, and φ_m and Φ_m are related to the convolution integral of the particle velocity and the pressure as, i.e., along X -axis,

$$\varphi_m(x, t) = \int_0^t \mathbf{u}_m(x, t') e^{-a_k(t-t')} dt' \tag{15}$$

The convolution terms in Equations (5), (6), (13) and (14) demonstrate that the material response is not instantaneous and accounts for the dispersion effects. Under the hypothesis of an immediate action–response material behavior, the integral contribution may be neglected, so (13) and (14) reduce to

$$\rho_{\infty} \frac{\partial \mathbf{u}_m}{\partial t} + \sum_{k=1}^{Np} A \mathbf{u}_m = -\nabla p_m \tag{16}$$

$$\frac{1}{\rho_{\infty} c_{\infty}^2} \frac{\partial p_m}{\partial t} + \sum_{k=1}^{Nc} B p_m = -\nabla \mathbf{u}_m \tag{17}$$

Either way, the discrete summation in Equations (16) and (17) should give a numerical real value, and thus, they may be replaced for a constant, frequency independent variable. In the same way, the asymptotic values of density and compressibility should have a real value that can be replaced with another numerical variable. Taking this hypothesis into account, the concepts of equivalent effective density, Ω , and equivalent effective compressibility, Ψ , can be introduced, as in Equations (1) and (2). The proposed Numerical Equivalent Acoustic Material (NEAM) characterizes porous materials through real values of numerical tortuosity, Ω_A , and numerical viscosity, Ω_B , both describing the viscous and inertial interactions, with the density being a value that depends solely on the propagation medium. Thereby, no asymptotic values must be used. Understanding that fluid-structure thermal exchanges may exist, due to frame elasticity and therefore compression-expansion changes, and there should also be some variables that can describe such behavior. Accordingly, the numerical compressibility, Ψ_A , and the numerical thermolabile, Ψ_B , could be introduced. As well, the static compressibility would just depend on the propagation medium. In the same way as the equivalent tortuosity and viscosity, the equivalent compressibility and thermolabile would not depend on the frequency either. As can be seeing in later sections, neglecting the convolution term does give acceptable results, and

characterizing a porous material without this term could explode the use of time domain methods. Then, after straight forward substitutions, Equations (16) and (17) can be reduce to the NEAM model as follows:

$$\Omega_A \frac{\partial \mathbf{u}_m}{\partial t} + \Omega_B \mathbf{u}_m = -\rho_0^{-1} \nabla p_m \tag{18}$$

$$\Psi_A \frac{\partial p_m}{\partial t} + \Psi_B p_m = -\rho_0 c^2 \nabla \cdot \mathbf{u}_m \tag{19}$$

Note that for values of $\Omega_A = \Psi_A \neq 0$, and $\Omega_B = 1, \Psi_B = 0$ for the NEAM model approach with the low frequency model, Equations (3) and (4), or the ZK model proposed by Van Renterghem et al., Equations (7) and (8). In addition, if $\Omega_A = \Psi_A = 1$, and $\Omega_B = \Psi_B = 0$, the NEAM leads to the linearized loss-less equations for momentum and mass conservation.

2.2. NEAM Model Coefficients

To estimate adequate values for NEAM model coefficients, $\Omega_A, \Omega_B, \Psi_A, \Psi_B$, input data from a material is needed. For that purpose, sound absorption coefficient, measured at normal incidence, and material thickness, are the only parameters that are required to calculate these coefficients. The proposed NEAM method requires simplicity, making it an appealing alternative for practical application. As there is some similarity between Equations (3), (4), (18) and (19), an initial parameters guess can be based on those from the low-frequency approximation. Afterwards, the simulated absorption coefficient is compared through an iterative optimization algorithm to the measured value in order to fit the equivalent values. Considering that the equivalent coefficients have to describe a comprehensive physical phenomenon, they are constrained for a non-multi-evaluated performance, as shown in Figure 1. Consequently, a simple linear gradient descent method could be used to find the function error minimum which, in this case, is an absolute minimum.

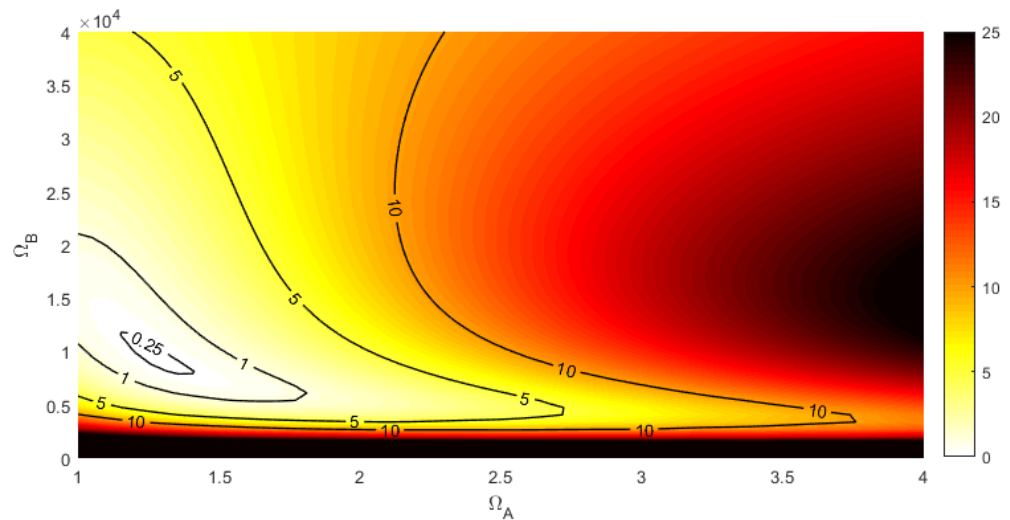


Figure 1. Computed space exploration for 1D simulation with a melamine foam porous absorber of 60 mm thickness. Figure shows the quadratic error, in percentage, with respect to input data measured in an impedance tube with ISO 10534-2 [28].

2.3. FDTD Method

Domain constitutive equations can represent a linear fluid without any losses, and may be described in terms of the Euler’s continuity equation and the momentum equation [29], respectively, as

$$\rho_0 \frac{\partial \mathbf{u}}{\partial t} = -\nabla p \tag{20}$$

$$\frac{1}{\rho_0 c_0^2} \frac{\partial p}{\partial t} = -\nabla u \tag{21}$$

To solve Equations (18) and (21), a classic FDTD method can be used, approximating the partial derivatives on constitutive equations using central finite differences schemes with staggered grids for the pressure and the particle velocity vector, both in space and time [30–32]. For example, in a 1D space along the X-axis, NEAM and domain momentum in Equations (18) and (20), respectively, with a first-order error, yield the next FDTD update equations

$$\left(1 + \frac{\Delta t \Omega_B}{2\Omega_A}\right) u_x|_{i+1/2}^{n+1/2} = \left(1 - \frac{\Delta t \Omega_B}{2\Omega_A}\right) u_x|_{i+1/2}^{n-1/2} - \frac{\Delta t}{\rho_0 \Delta x \Omega_A} (p_x|_{i+1}^n - p_x|_i^n) \tag{22}$$

$$u_x|_{i+1/2}^{n+1/2} = u_x|_{i+1/2}^{n-1/2} - \frac{\Delta t}{\rho_0 \Delta x} (p_x|_{i+1}^n - p_x|_i^n) \tag{23}$$

where subscript “n” denotes time steps an “i” space steps. The same goes for the other update equations.

Since the simulation domain has finite dimensions, a useful working space has to be limited to ensure that reflections do not disturb the interest region. To avoid such spurious reflections, a perfectly match layer (PML) is used according to [31]. Algorithm stability is given by the Courant–Friedrich–Levy (CFL) condition, from which is defined the critical time step that ensures information propagation between cells. In a 2D Cartesian coordinates system, CFL condition is established as in [32]. Since an equally-spaced square grid is used, spatial increments are the same in both directions, and so, CFL condition is simplified. To setup a simulation, the minimum points per wave length (PPWL) must be defined to provide an adequate signal and domain resolution. Then, given a maximum CFL number and minimum PPWL, it is possible to calculate spatial and temporal increments to ensure stability.

2.4. FDTD Setup

One-dimensional and two-dimensional FDTD schemes were used to compute normal and oblique incidence, respectively. Simulations were performed with 20 PPWL, considering an upper frequency of $4\text{ k}\sqrt{2}$.

Normal incidence evaluation is the first step in NEAM modeling algorithms. On one hand, its goal is to compare simulated absorption coefficients with measurements performed in an impedance tube, according to ISO 10534, parts I and II [28,33]. On the other hand, the aim is to determine the equivalent coefficients that are to be used in 2D FDTD simulations (oblique incidence). The algorithm uses a summed multiple Ricker wavelet as input signal, which was developed to obtain a flat frequency response ranging from 125 Hz to 4 kHz octave bands. A signal with a summed ripple < 1.6 dB in the interest region is obtained. The FDTD air domain is computed with the linearized Equations (20) and (21). A quadratic PML was used on one side of the FDTD domain, and, on the other tube side a NEAM was placed with an impervious wall behind. One receiver captures the input and reflected pressure to and from NEAM, namely p_I and p_R . Afterwards, incident and reflected components can be obtain by an adequate time windowing, acquiring then, via transfer function, the complex reflection factor as $R = \text{FFT}\{p_R\} / \text{FFT}\{p_I\}$, where FFT is the Fast Fourier Transform acronym. Following that, normal incidence absorption coefficient is calculated as $\alpha_n = 1 - |R|^2$ [34]. In addition, material surface impedance is extracted from FDTD results as the pressure to the particle velocity ratio at NEAM interface.

A similar approach is conducted for the 2D FDTD procedure. In this case, oblique incidence is computed, obtaining, from individually angled simulations, the random incidence sound absorption thanks to Paris’ integration [35]. The use of the oblique incidence in the 2D FDTD method was taken into account to quantify if the 1D virtual coefficients (normal incidence) could also settle the diffuse behavior. To evaluate the signal incidence angle, periodic boundary conditions were implemented at the top and bottom

of the 2D domain using the sine–cosine method expressed in [31]. A PML layer is used in X-direction to prevent unwanted reflections at the domain beginning. Also, a NEAM is placed at the end of the domain with a rigid backing. Figure 2 shows the 2D domain simulation scheme. As the 2D model has periodicity in the Y direction, the NEAM behaves like an infinite material. Consequently, ISO 354 measurements [36], which are based in finite size samples, should not be used to compare absorption coefficient results. Instead, analytical calculations for infinity samples must be chosen. Since periodic boundaries are frequency dependent, the Ricker wavelet is no longer used. As an alternative, sinusoidal waves, centered at one third octave bands from 100 Hz to 5 kHz, are employed. Finally, the absorption coefficient is evaluated using the standing wave method expressed in ISO 10534-1.

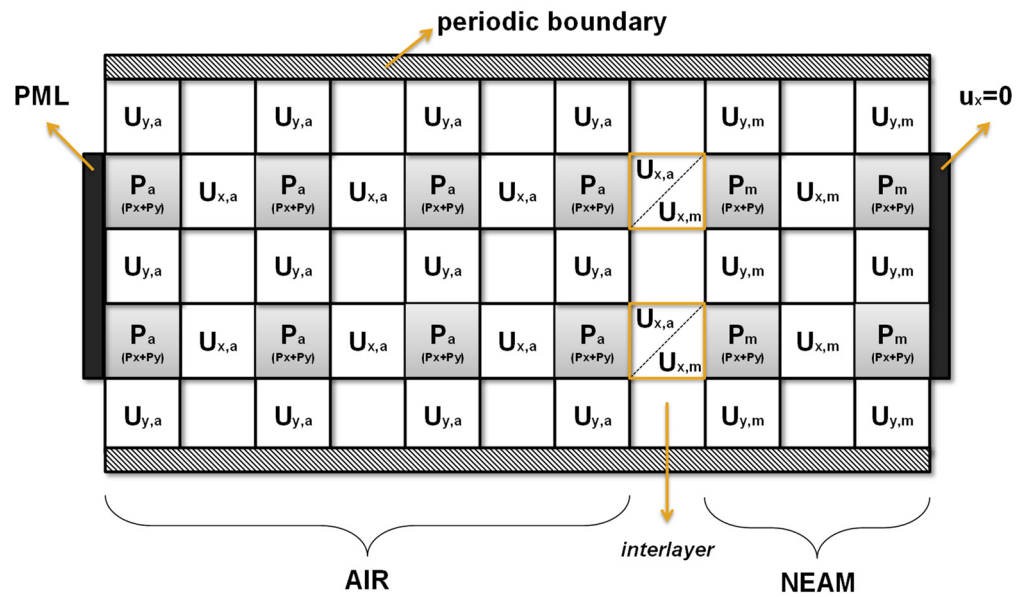


Figure 2. The 2D FDTD domain schemes where all constraints are placed. Subscript “a” denotes air, “m” indicates material, “x” propagation along x-direction and “y” propagation along y-direction.

2.5. Experimental Setup

Considering that this report focuses on the FDTD NEAM model development, materials absorption coefficients were selected from others scientific reports. Nevertheless, as it was shown in previous sections, the model simplicity only requires the absorption coefficient measured in an impedance tube, which can be calculated with ISO 10534 standard. Thus, the present work presents just two measures of the absorption coefficient, one for a porous absorber [37], and the other for PET fibers [38], later described in Sections 3.1 and 3.2.

3. Results

In this section, the results obtained through FDTD simulations are summarized. The NEAM model has been calibrated for several materials, illustrating the algorithm applicability to different situations. In fact, although the model was created to model the macroscopic behavior of porous absorbers, as it is adaptive, it may also work with other kinds of kernels, such as fiber ones. Accordingly, one porous absorber and one fiber material were computed to compare their results with those measured or analytically calculated. Figure 3 shows each material at microscope resolution, seeing their kernel differences. For each material, sound absorption at normal and random incidence is presented. Additionally, normal incidence surface impedance is also shown. For the purpose of a better modeling resolution, FDTD absorption coefficient and measurement data were taken in one third octave bands from 100 Hz to 5 kHz. All simulations were handled with Matlab in a six core AMD Ryzen 5 4500 U processor at 3.40 GHz and 32 GB DDR4 RAM. The average usage was

75% for CPU and 35% for RAM. Section 3.1 presents the numerical results obtained for a 60 mm melamine foam sheet (porous kernel). In Section 3.2 are analogous results with a 40 mm PET sheet (fibrous kernel). In Section 3.3, the NEAM model is used to extract the low-frequency approximation parameters from a porous material, which are the tortuosity and the viscosity. Finally, Section 3.4 summarizes the NEAM performance through a series of tests that determine the method strength.

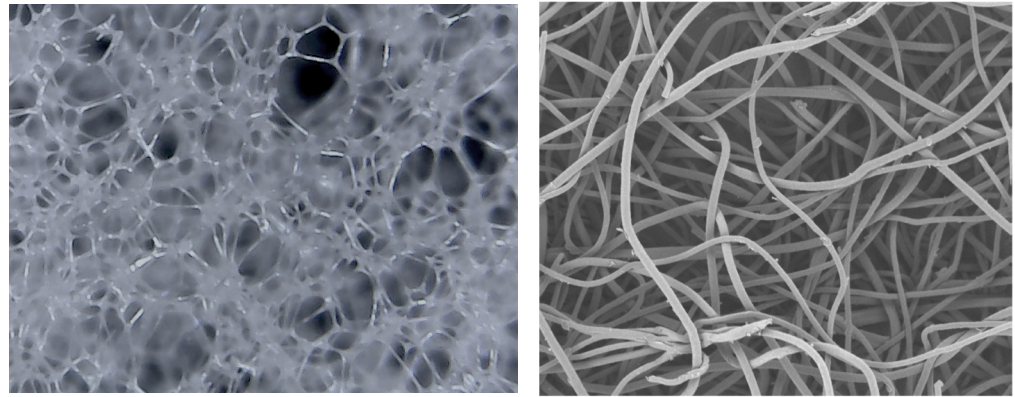


Figure 3. Microscopic kernel differences on the studied materials, although the computed behavior is macroscopic. **Left:** Melamine foam (image by the authors); **Right:** PET fiber, from [38] gently provided.

3.1. Porous Melamine Foam

Melamine foam is a formaldehyde–melamine–sodium copolymer made of melamine resin. Due to its absorptive capacity and flame-retardant ability, its use is extensive in building acoustics as an absorbing material. In Reference [37], material absorption results are presented for a 60 mm sheet, and so they are taken here as a reference for comparison with the NEAM model.

Figure 4 shows a normal absorption coefficient resulting from the 1D FDTD simulation scheme, which are, indeed, very similar to the measured ones. Below 315 Hz, there is an overestimation of sound absorption with a maximum deviation at 125 Hz of 0.06. Variation could be due to the fact that normal incidence measures below 315 Hz may have an inherent error caused by the tube length. As far as the authors' knowledge, no setup conditions were presented in Reference [37]. In addition, a mismatch is noticeable at 4 kHz and 5 kHz. This particular error can be accounted for the one third octave band average done to the FDTD continuous values. As perceived, averaged values cannot follow the continuous ripple, and so certain values are lost, yielding a flat sound absorption response from 3150 Hz to 5000 Hz, which would not exist in the original FDTD calculation. Figure 5 presents the normal incidence surface impedance, where it can also be seen a good agreement with the analytical result calculated with the JCAL model. At high frequencies above 2 kHz, there is a slight deviation with the 2D FDTD results, which can be accounted for two reasons: (a) In Figure 4, normal incidence sound absorption is also a mismatch at the 2 kHz band, which increases the absorption, meaning that the impedance should be also higher. (b) The FDTD method dispersion could deviate these peak frequencies. At low frequencies, the material is purely reactive and capacitive, similar to an electrical open circuit, where voltage (pressure analogous) is maximum and no pressure drops through the material. Diffuse sound absorption is presented in Figure 6. It reflects a strong similarity with the analytical data. As well as for 1D FDTD results, there is a deviation at high frequencies. However, the total error made is insignificant. At low frequency, the comparison holds, differentiating from the 1D model because it takes into account different angles of incidence, and therefore, the absorption coefficient final response is smoothed all over.

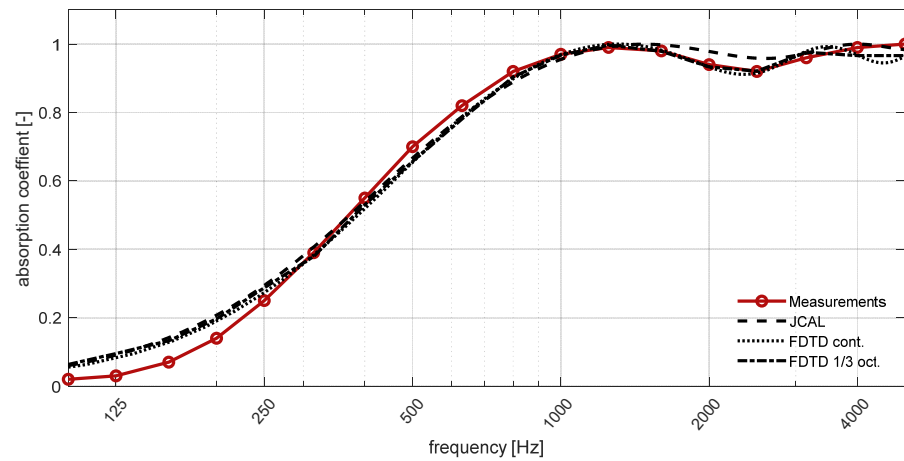


Figure 4. The 60 mm melamine foam normal incidence sound absorption computed with 1D FDTD scheme compared with ISO 10534 measurements (red line), black line is the FDTD full calculation, and blue line is the black line averaged to 1/3 octave bands.

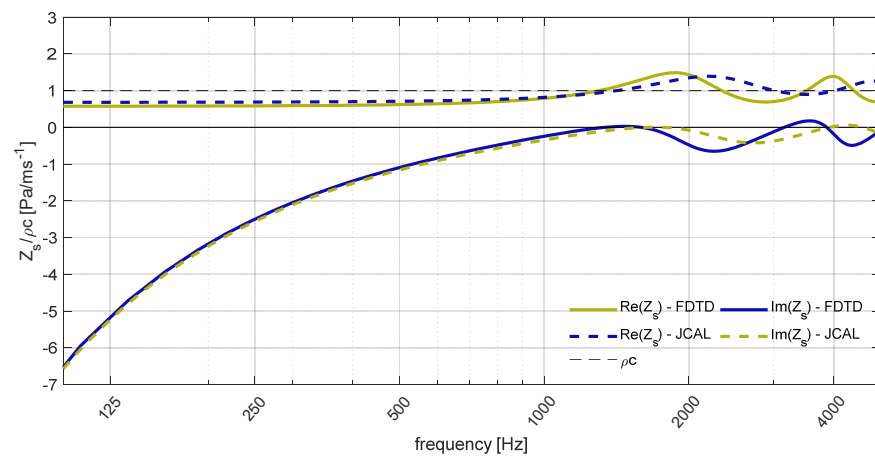


Figure 5. The 60 mm melamine foam surface impedance at normal incidence computed with 1D-FDTD scheme.

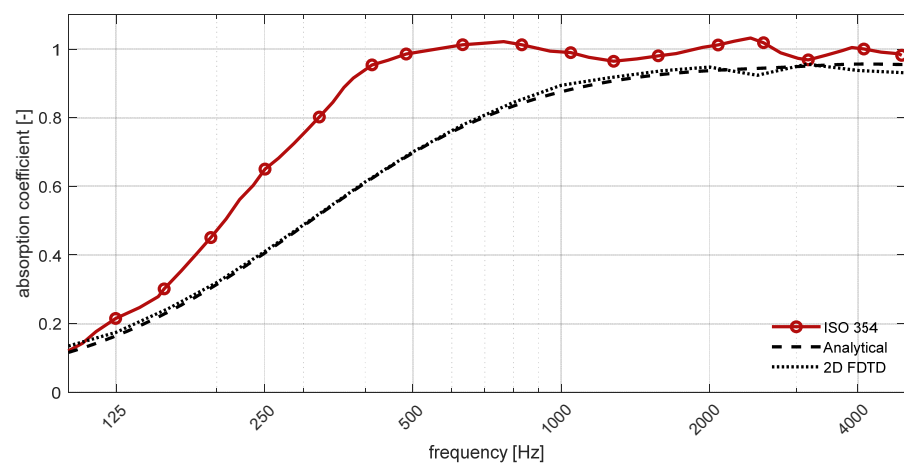


Figure 6. The 60 mm melamine foam diffuse field calculated using oblique incidence absorption and Paris' formulation.

3.2. PET Fiber Sheet

Poly-Ethylene Terephthalate (PET) is a polymer made from polyester resin. Its use is also commonly extended because most of it is made of recycled plastics. In Reference [38],

a series of PET fiber sheets were tested, discerning between pure and recycled PET. The acoustic behavior of this type of materials is characterized by a soft absorption, normally at high frequencies. Here, the recycled 40 mm and 1.2 kg/m² PET sheet normal incidence sound absorption is compared. As in Reference [38], there are no macroscopic parameters for the JCAL model, a reverse engineering method was employed to extract these five parameters from the absorption coefficient. Figure 7 shows a good agreement between 1D FDTD sound absorption and measurements. The reverse JCAL results vary at low frequencies below 315 Hz. In consequence, less absorption is calculated. Figure 8 displays the normal incidence surface impedance. A capacitive behavior is observed at low frequencies, as for the porous absorber. Nevertheless, below 250 Hz, the real part increases in the 2D FDTD result. Given that, the material absorption is also increased. At high frequencies there is a minor deviation at the peak frequency, which may be a result of FDTD dispersion. Regardless, comparison between the NEAM model results and the analytical data is accurate. Finally, Figure 9 shows the diffuse sound absorption with a great alignment with theoretical data. Frequencies beneath 315 Hz also show a sound absorption excess compared to the analytical data. As the JCAL model was implemented for porous absorption, it cannot be assured that the observed behavior is wrong. From the theoretical calculation in 1D, it is observed that, for low frequency, the NEAM model adjusts to the parameters measured in the impedance tube, while the JCAL model underestimates the absorption. Since the same parameters are used for diffuse calculation, the error made could have propagated to the results, thus, differing from the FDTD results.

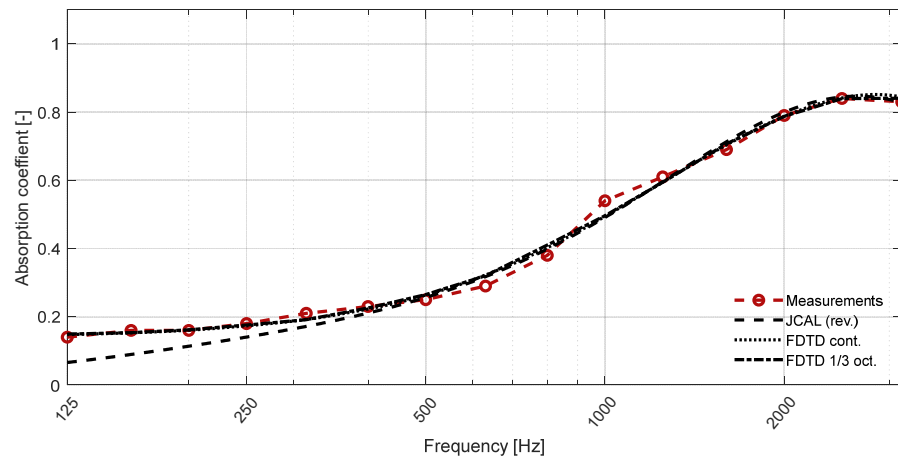


Figure 7. The 40 mm PET sheet normal incidence sound absorption computed with 1D FDTD scheme compared with ISO 10534 measurements (red line); black line is the FDTD full calculation, and blue line is the black line averaged to 1/3 octave bands.

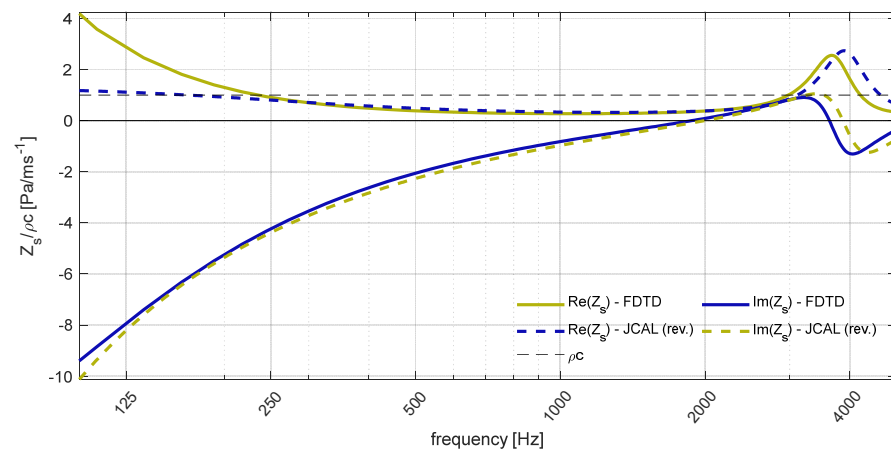


Figure 8. The 40 mm PET surface impedance at normal incidence computed with 1D-FDTD scheme.

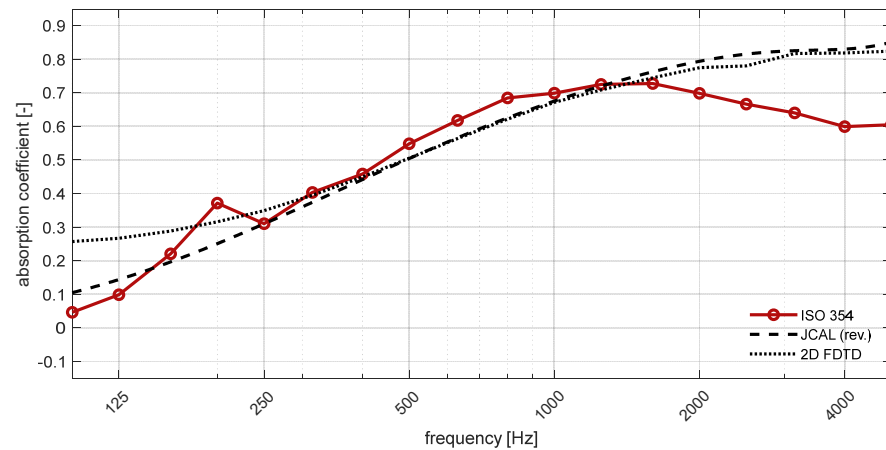


Figure 9. The 40 mm PET diffuse field calculated using oblique incidence absorption and Paris formulation.

3.3. NEAM Use to Extract Physical Parameters

Seeing the similarity between the NEAM model and the low-frequency approximation model, it should be possible to relate the physical material parameters using the coefficients obtained with NEAM. To verify this relation, Equations (3) and (4) have been programmed into the 1D FDTD scheme, creating a non-physical material to calculate the absorption coefficient. The proposed non-physical material characteristics are presented in Table 1. Results obtained from the 1D FDTD NEAM model for different PPWLs are then compared to the low frequency model and gathered in Table 2.

Table 1. Properties for a virtual material which are used to calculate the absorptive performance with the low frequency model in 1D FDTD scheme.

α_{∞} [-]	K_0 [Pa]	η [Pa·s]	ϕ [-]	th. [mm]
1.0953957103 ¹	9×10^{-10}	18×10^{-6}	0.98	50

¹ Obtained from local theory.

Table 2. Results obtained with 1D FDTD NEAM model using diverse PPWL. NEAM results are compared to the low frequency model results in order to extract the true values from Table 3.

PPWL	Ω_A Rounded	Ω_A Not Rounded	Ω_B Rounded	Ω_B Not Rounded
6	1.0000017548	1.0000017548	13,833	13,790
10	1.0390070343	1.0301187897	18,225	18,582
20	1.0419824982	1.0337904358	18,395	18,728
30	1.0826280975	1.0741842651	19,084	19,429
40	1.1039675140	1.0953920746	19,450	19,800
low. freq. model	1.0953957103		19,800	

In this example, as can be observed in Equations (4) and (19), when $\Psi_A = 1$, $\Psi_B = 0$ thermal effects are neglected, that the NEAM model simplifies to just viscous effects. Furthermore, as follows in the document, the low-frequency approximation of tortuosity is directly related to the Ω_A NEAM coefficient, which should yield similar result, and the effective flux resistivity $\eta\phi/k_0$ is also directly related to the Ω_B NEAM coefficient. The low-frequency parameters were calculated with the 1D FDTD schemes with 40 PPWL, and the absorption coefficient solution, which is the input data for the NEAM model block, was considered with and without rounding decimals. The “rounded” data entry in Table 2 has been estimated with two significant figures.

3.4. Algorithm Performance

As the FDTD setup remains constant for all material simulations, performance results are very similar. Therefore, the full performance here is only described for the 60 mm sheet of melamine foam. Due to the exponential growth of the time spent in low-frequency simulations, discussed later in a dedicated section, performance studies were conducted from 315 Hz to 5 kHz for 2D FDTD simulations.

In Section 3.4.1 are shown the Paris' formulae usage limitations for the absorption coefficient calculation at oblique incidence. Section 3.4.2 presents the NEAM model behavior using different PPWLs, which can be useful in order to reduce computational time. Section 3.4.3 covers how spatial tube dimensions affect the absorption coefficient simulation. Section 3.4.4 studies the minimum simulation time needed to accurately record the pressure inside the tube at every frequency and every incidence angle. Also, an algorithm stop criteria is given. At last, in Section 3.4.5, computational costs can be observed using the above machine.

3.4.1. Paris Integration Domain

As previously explained, random incidence sound absorption is calculated using Paris' integration formula with a selected range of angles. As a consequence, the angular step may affect the final result. Figure 10 presents diverse integration steps in the range $[0-90^\circ]$. As Paris' equation has a sinusoidal term in it, angles of 0° and 90° have no weight when diffuse field absorption is calculated. Given this circumstance, 0° and 90° simulations were not computed, thus saving computational time. The figure illustrates the effect of adopting different angle steps in the estimation of the random incidence sound absorption, clearly showing that a 10° step is enough to accurately perform this calculation.

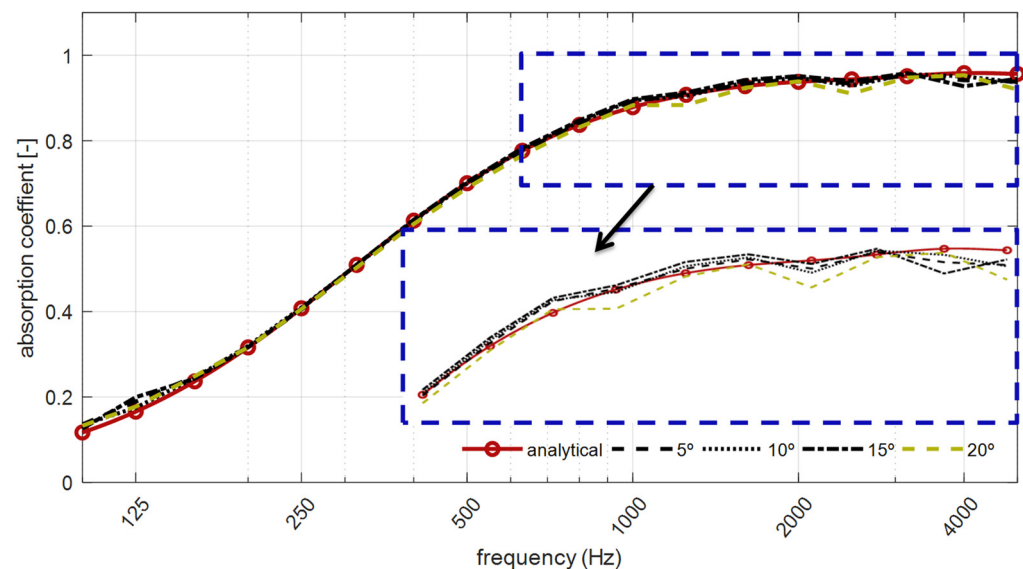


Figure 10. Diffuse absorption coefficient calculated for a 60 mm melamine sheet using oblique incidence with Paris' formulation using different angle integration steps. The insert shows a zoomed area from 630 Hz to 5 kHz and absorption coefficient amplitude from 0.7 to 1.

An additional condition of Paris' formula is the integration limits, which are also defined by nature from 0 to 90° . Figure 11 shows the differences when choosing several integration limits summarized in Table 3, with a 5° step and, as suggested in Reference [35], the case in which only the calculation at 55° is carried out for locally reactive materials is also compared. The figure shows good agreement with analytical data, so Paris' integration can be performed with a 10° to 80° range, with 10° steps, without losing information.

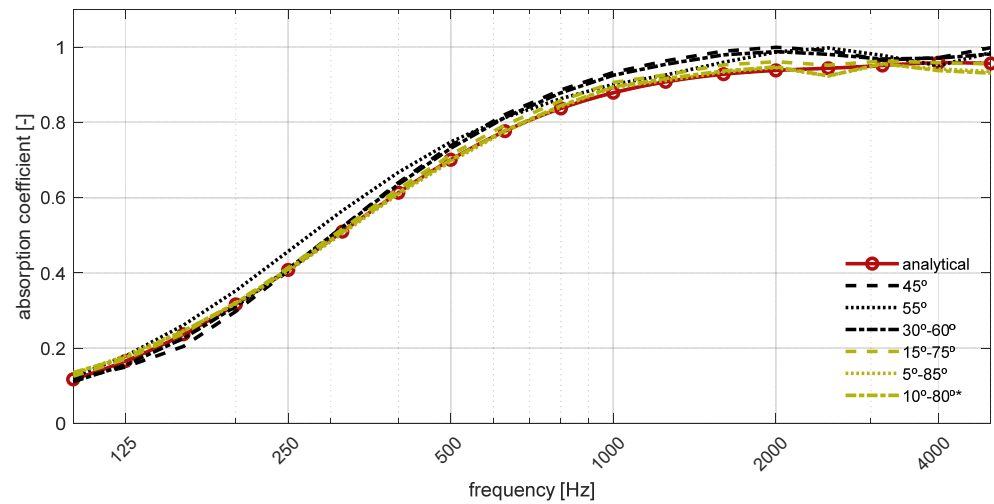


Figure 11. Diffuse absorption coefficient calculated for a 60 mm melamine sheet with Paris’ formulae using the different angle ranges from Table 3. * Range calculated with 10° step.

Table 3. Evaluation of the total information at Paris’ formulae to perform absorption calculation depending on the input angle ranges, calculated with a 5° step.

Angles Range [°]	Weight at Paris’ Integration [%]
45	8.8
55	8.2
30–60	57.6
15–75	90.1
05–85	100.0
10–80 ¹	100.0

¹ Range calculated with 10° step.

3.4.2. Minimum PPWL

This study is conducted to show absorption coefficient results using different PPWL configurations for 1D and 2D schemas. Figure 12 shows the different PPWL values chosen at the 1D FDTD scheme compared to measurements values in Kundt tube. As seen in the figure, no differences can be observed. As a consequence, just for the 1D case, even the minimum value of 6 PPWL yields good results. As NEAM modeling is adaptive to the given input data, and a set of fixed FDTD parameters, 1D FDTD absorption coefficient results shall not vary, thus varying the NEAM coefficients values only. In fact, just mixing combinations between 1D and 2D PPWL will yield different results.

The four NEAM coefficient results are extracted from the 1D FDTD, which are used in the 2D simulations. Then, just downscaling PPWL interactions between 1D NEAM coefficients to 2D ones were simulated, outlined in Table 4 and represented in Figure 13.

Table 4. PPWL used at 1D-FDTD calculation downscaled to 2D FDTD to compute the absorption coefficient.

1D PPWL		2D PPWL			
30	30	20	10 ¹	6 ¹	6 ¹
20		20	10 ¹	6 ¹	6 ¹
10		10 ¹		6 ¹	
6			6 ¹		

¹ X and Y dimensions are doubled due to the low space grid quantity, guaranteeing correct propagation.

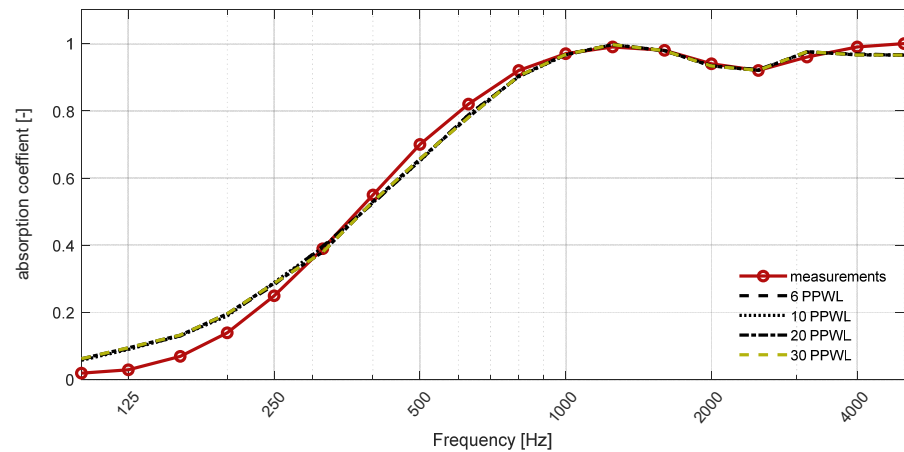


Figure 12. Measured normal incidence sound absorption compared to 1D FDTD simulations using different PPWL values for a 60 mm melamine sheet.

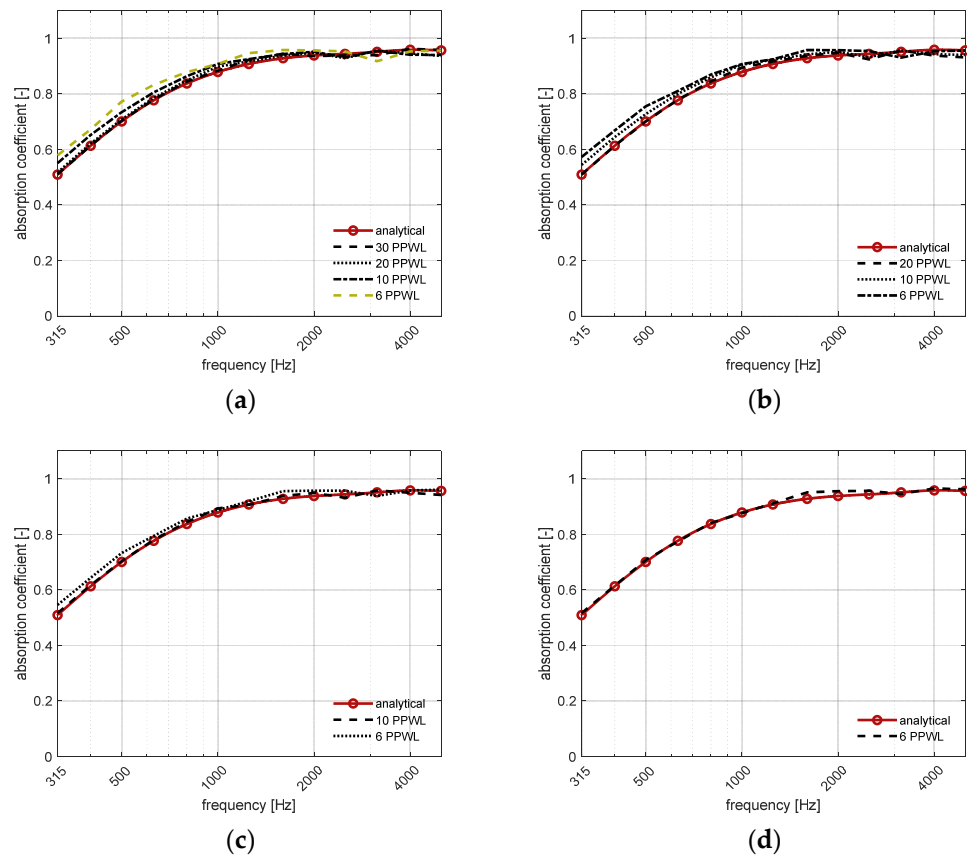


Figure 13. The 60 mm melamine sheet sound absorption calculated with JCAL model and compared to 2D FDTD simulations using downscaled PPWL factors from Table 4. The 1D NEAM coefficient values are calculated at (a) 30 PPWL, (b) 20 PPWL, (c) 10 PPWL, (d) 6 PPWL.

Figure 13 shows that the relationship between PPWL and the result performance holds, regardless of the number of points chosen, as for the 1D case. Knowing that the equivalent coefficients are adaptive and do not seek to be related to physical principles, reducing the number of PPWLs would increase the number of calculations performed, or the volume of the FDTD mesh, thus improving the computational performance.

3.4.3. Domain Dimensions

It is well-known that a much larger space has more computational cost, and therefore, it is recommended to seize computational resources. The next study shows how different dimensions affect the final absorption coefficient. The algorithm was programmed to have at least two nodes inside the tube at every frequency and every incidence angle. For that, domain length is incremented at $\lambda_0/\cos(\theta)$ ratio. For Y-direction, Figure 14 shows different simulations varying Y-space according to wavelength multiples, these being $\lambda_0, \lambda_0/4, \lambda_0/2, 0.58\lambda_0$, and their combinations with $\cos(\theta)$ ratio. As there is no tendency change, the next figure just shows the cases in which the behavior is different. It can be observed that the choice of the Y-dimension does not affect the final result as long as the mesh is sufficiently representative. Just for $\lambda_0/4$ the absorption coefficient has been altered. For convenience a $0.58\lambda_0$ factor was selected as in ISO 10534.

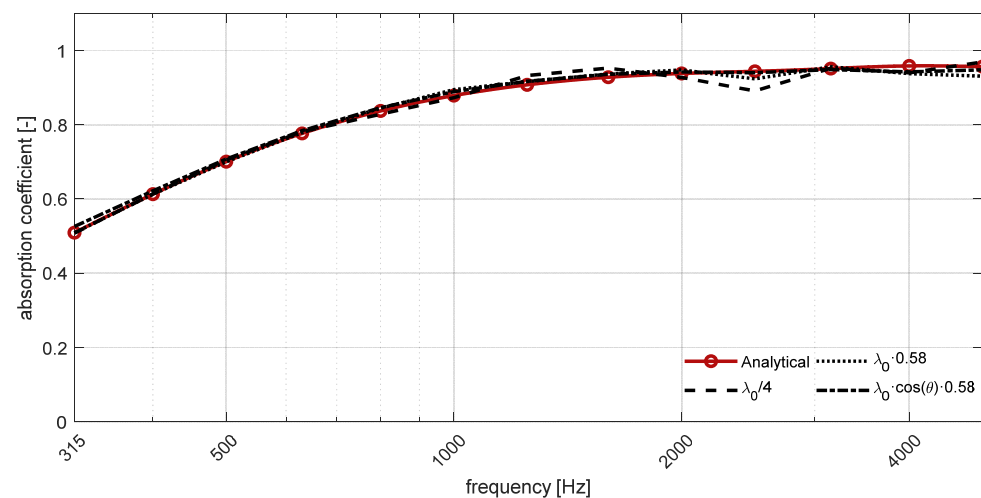


Figure 14. The 60 mm melamine sheet sound absorption at random incidence using different domain widths (Y-direction) and a constant value of X-space set to $\lambda_0/\cos(\theta)$.

3.4.4. Propagation Time

In previous sections, it was already explained that the 2D FDTD calculation needs a sinusoidal input signal due to the periodic boundaries. One main problem of this configuration is the time that the signal needs to spread completely at high incidence angles, as can be seen in Figure 15, where space–time plots are presented. Before signal stabilization, a ripple effect is visible in the plots.

With a view to avoid this ripple, and possible pressure voids, simulation time can be increased in order to adequately stabilize the pressure response.

Figure 16 shows the error made at 250 Hz, 500 Hz and 1 kHz absorption calculation at different angles as a function of the simulation time. It can be seen that for low angles, the absorption coefficient becomes accurate in most cases, after a simulation time below 50 ms. For higher angles, the ripple effect becomes noticeable, but increasing propagation time helps to stabilize the pressure so that convergence to the final absorption coefficient can be reached within a given tolerance. To help in the analysis, the reception signal may be averaged for the last milliseconds of each simulation, avoiding the initial time where the signal did not reach the NEAM interface, and to prevent possible spatial pressure variations. In the Figure 16 plots, mean squared error (MSE) variation in the absorption coefficient estimation is shown as a function of the simulation time, clearly revealing that the error is progressively reduced and that the absorption coefficient converges to the measured value. For higher angles, these curves are clearly more oscillatory, indicating that the convergence process is more irregular, although convergence is still reached. To allow a better evaluation of a possible convergence criterion, avoiding the effect of those oscillations, a smoothed MSE curve was also computed (figure green lines). Making use of this approach, even for the more challenging case presented (1 kHz and 80°), it is possible to

evaluate a convergence criterion with simplicity and select the stop point in the simulation process based on this criterion.

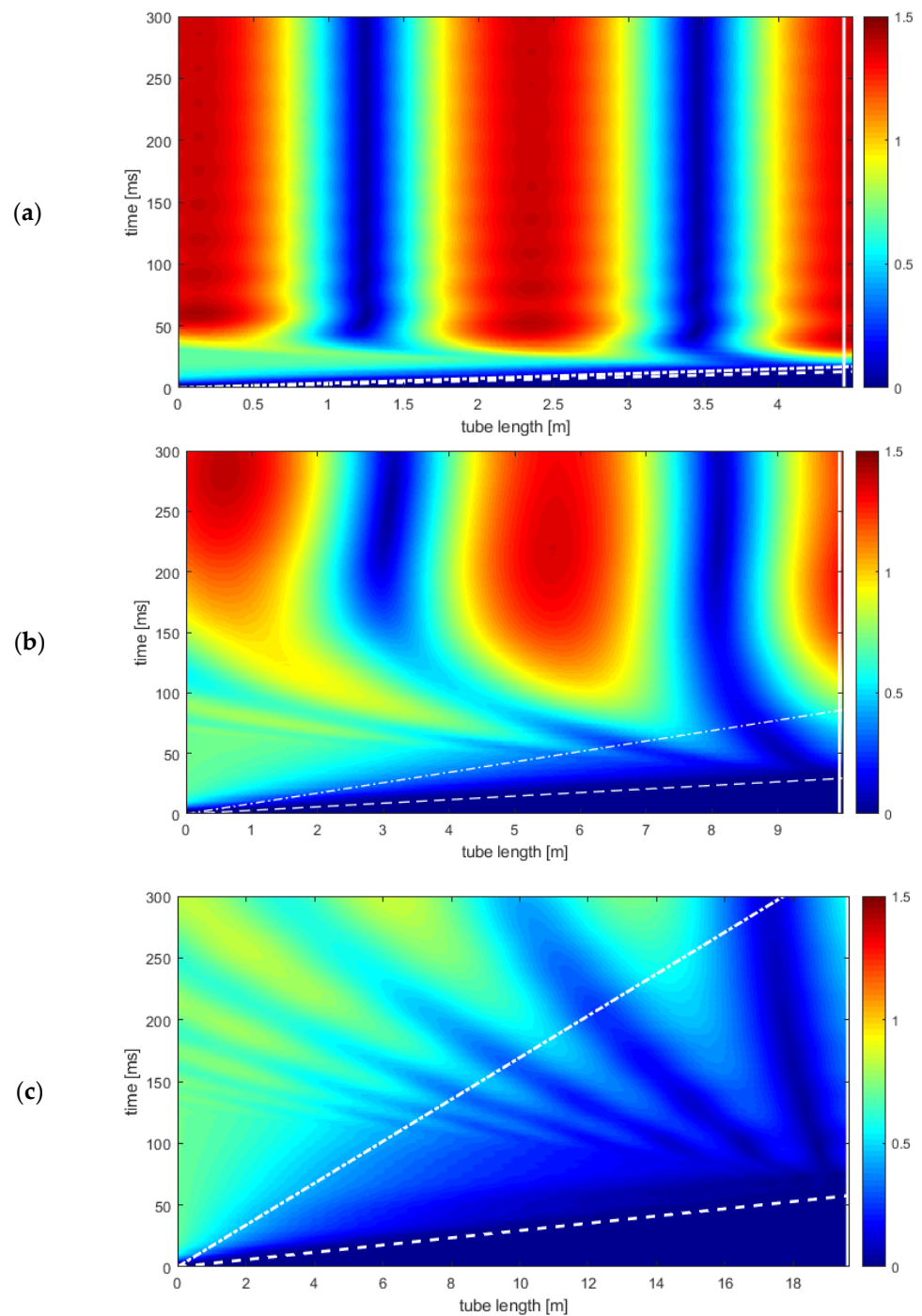


Figure 15. Space–time plots for a 60 mm melamine sheet at 100 Hz and different incidence angles. Absolute pressure values are represented with [0–300] ms time interval and different incidence angles, (a) 40°, (b) 70°, (c) 80°. White continuous line represents the first NEAM layer, dashed line C_0 , and dotted-dash $C_0 \cdot \cos(\theta)$. Note that the tube length increases with the incidence angle.

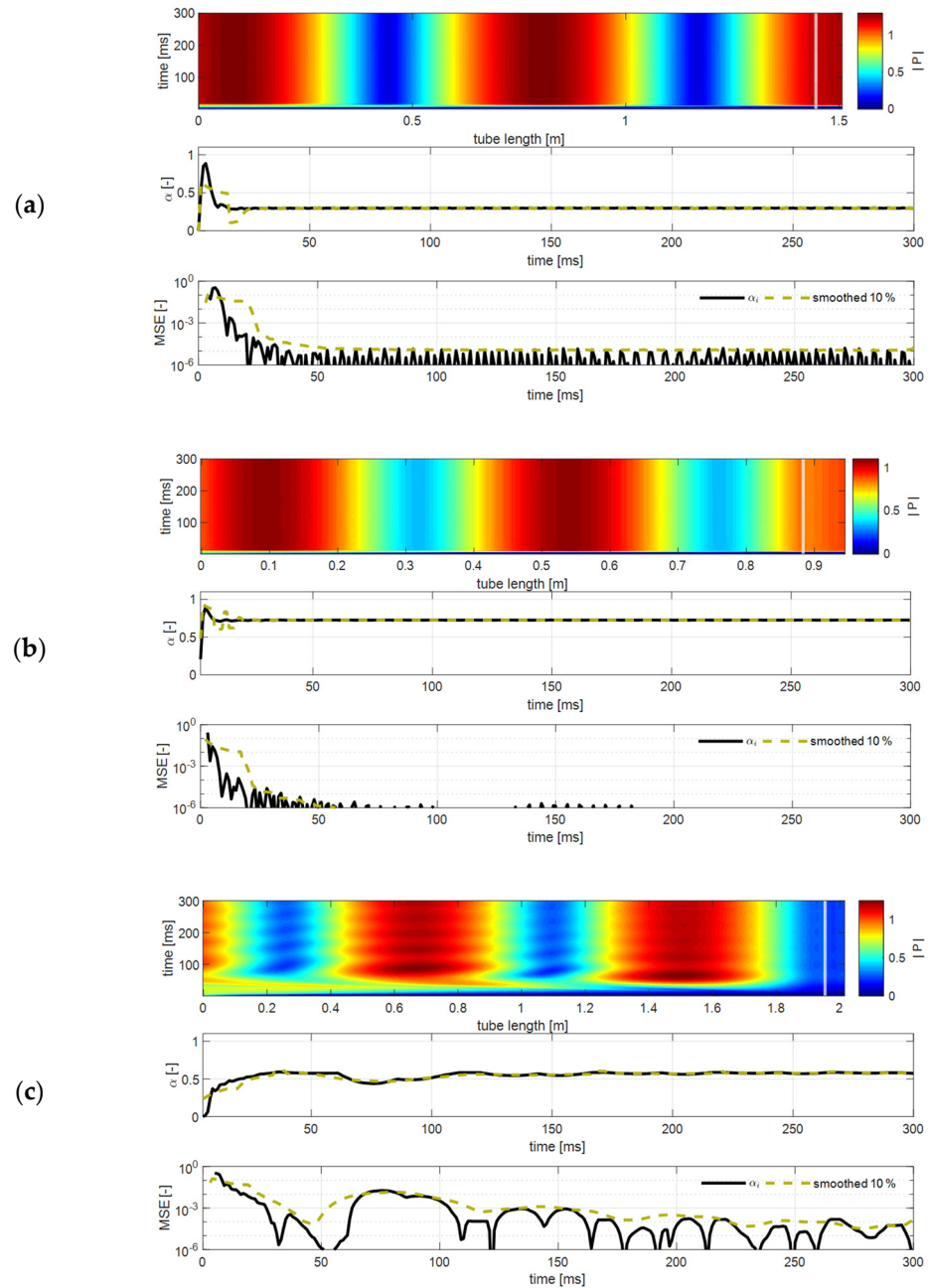


Figure 16. Each figure, computed for a 60 mm melamine sheet, is divided in three rows: (1) Absolute space–time pressure. (2) Diffuse absorption coefficient calculated using different true values. (3) Mean Squared Error (MSE) with the black line representing the error using the last time pressure to calculate the true value of the absorption coefficient, and dotted green line a 10% sample smooth with an average of the last 150 ms as the true value. The different cases shown correspond to (a) 250 Hz at 20° , (b) 500 Hz at 40° , (c) 1 kHz at 80° .

Figure 17 shows the propagation time needed for an entire simulation with an MSE of 10^{-3} as a stop criterion. In this color plot, in which white and black shades correspond, respectively, to smaller and higher simulation times, it is clear that, except for very high incidence angles and low frequencies, simulation times below 50 ms are sufficient to obtain the required tolerance.

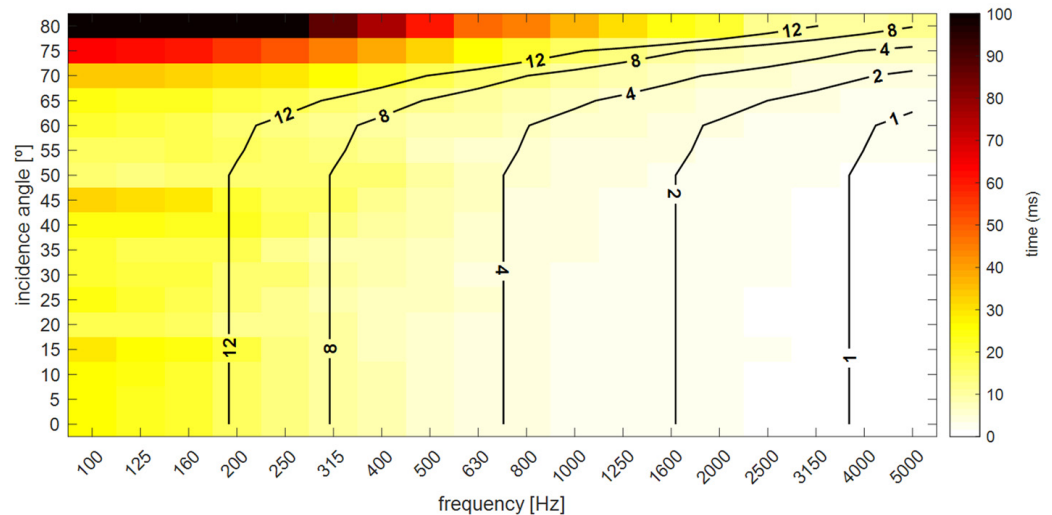


Figure 17. Minimum propagation time needed to compute the diffuse field sound absorption coefficient of a 60 mm melamine sheet, for each angle and frequency, with an error of 10^{-3} . True value of alpha was calculated with an average of the last 150 ms calculation. Black lines delineate time limits in milliseconds.

3.4.5. Computing Time

An important aspect of algorithm performance is the time needed to complete a full material study, using 2D FDTD at 20 PPWL for the full frequencies range, considering calculations for all angles. For frequencies ranging from 315 Hz to 5 kHz the total time taken by the algorithm was 15 h. Underneath 315 Hz, and for high angles, computing time increases dramatically, with a total of 212 h just for the 100 Hz to 315 Hz range. Since a much larger simulation space is required for high angles and low frequencies, computational costs become extremely high.

4. Conclusions

As it has been possible to verify, throughout this document, that a fluid-like linear propagation model for absorbent materials has been achieved, which can be adapted to the most common types of nuclei, such as pores and fibers. The model shows a strong correlation between the measurements carried out in the laboratory with the results obtained by the FDTD method. It has been shown that with a single measurement of the absorption coefficient at normal incidence, the model is able to accurately characterize the material frequency response. In addition, with the method used, other material characteristics can be obtained, such as the surface impedance and the diffuse absorption coefficient. The 2D FDTD method also achieves good agreement with the analytical data for an infinite sample, and it remains a riddle if the 1D FDTD coefficient values can be used for 3D simulations. It also has been verified that computation time can be optimized by decreasing the PPWL number, without counteracting the absorption coefficient characterization. Nevertheless, downsizing PPWL ratio results in the loss of physical information related to the material. The NEAM model equations simplicity can extend their use to different fields within acoustics in which the time domain response of porous materials is relevant, for instance, room acoustics. However, due to the lack of information, it cannot be guaranteed that the method is reliable at frequencies below 315 Hz, noting, a priori, a slight overestimation of the absorption coefficient.

Author Contributions: P.C.I.: Conceptualization, methodology, software, validation, formal analysis, investigation, data curation, writing—original draft, visualization; L.G.: methodology, validation, writing—review and editing; J.R.: methodology, validation, writing—review and editing, supervision. All authors have read and agreed to the published version of the manuscript.

Funding: This work was supported by the Spanish Ministry of Economy and Innovation (MINECO) and the European Union FEDER (project PID2019-109175GB-C22). This work was partly financed by FCT/MCTES through national funds (PIDDAC) under the R&D Unit Institute for Sustainability and Innovation in Structural Engineering (ISISE), under reference UIDB/04029/2020 (doi.org/10.54499/UIDB/04029/2020), and under the Associate Laboratory Advanced Production and Intelligent Systems ARISE under reference LA/P/0112/2020.

Institutional Review Board Statement: Not applicable.

Informed Consent Statement: Not applicable.

Data Availability Statement: All data used in this document can be generated by following the steps mentioned in Section 2.

Conflicts of Interest: The authors declare that they have no known competing financial interests or personal relationships that could have appeared to influence the work reported in this paper.

References

1. Attenborough, K. Acoustical characteristics of porous materials. *Phys. Rep.* **1982**, *82*, 179–227. [[CrossRef](#)]
2. Biot, M.A. Theory of propagation of elastic waves in a fluid-saturated porous solid. I. Low-frequency range. *J. Acoust. Soc. Am.* **1956**, *28*, 168–178. [[CrossRef](#)]
3. Biot, M.A. Theory of propagation of elastic waves in a fluid-saturated porous solid. II. Higher frequency range. *J. Acoust. Soc. Am.* **1956**, *28*, 179–191. [[CrossRef](#)]
4. Delany, M.E.; Bazley, E.N. Acoustical properties of fibrous absorbent materials. *Appl. Acoust.* **1970**, *3*, 105–116. [[CrossRef](#)]
5. Fellah, Z.E.A.; Depollier, C. Transient acoustic wave propagation in rigid porous media: A time-domain approach. *J. Acoust. Soc. Am.* **2000**, *107*, 683–688. [[CrossRef](#)] [[PubMed](#)]
6. Fellah, M.; Fellah, Z.E.A.; Depollier, C. Generalized hyperbolic fractional equation for transient-wave propagation in layered rigid-frame porous materials. *Phys. Rev. E* **2008**, *77*, 016601. [[CrossRef](#)] [[PubMed](#)]
7. Lafarge, D.; Lemarinier, P.; Allard, J.F.; Tarnow, V. Dynamic compressibility of air in porous structures at audible frequencies. *J. Acoust. Soc. Am.* **1997**, *102*, 1995–2006. [[CrossRef](#)]
8. Johnson, D.L.; Koplik, J.; Dashen, R. Theory of dynamic permeability and tortuosity in fluid-saturated porous media. *J. Fluid Mech.* **1987**, *176*, 379–402. [[CrossRef](#)]
9. Jaouen, L.; Gourdon, E.; Glé, P. Estimation of all six parameters of Johnson-Champoux-Allard-Lafarge model for acoustical porous materials from impedance tube measurements. *J. Acoust. Soc. Am.* **2020**, *148*, 1998–2005. [[CrossRef](#)]
10. Niskanen, M.; Groby, J.-P.; Duclos, A.; Dazel, O.; Le Roux, J.C.; Poulain, N.; Huttunen, T.; Lähivaara, T. Deterministic and statistical characterization of rigid frame porous materials from impedance tube measurements. *J. Acoust. Soc. Am.* **2017**, *142*, 2407–2418. [[CrossRef](#)]
11. Cortis, A. Dynamic Acoustic Parameters of Porous Media. Ph.D. Thesis, Technische Universiteit Delft, Delft, The Netherlands, 2002.
12. Horoshenkov, K.V.; Hurrell, A.; Groby, J.-P. A three-parameter analytical model for the acoustical properties of porous media. *J. Acoust. Soc. Am.* **2019**, *145*, 2512–2517. [[CrossRef](#)]
13. Kosten, C.W.; Zwikker, C. *Sound Absorbing Materials*; Elsevier: Amsterdam, The Netherlands, 1949.
14. Escolano, J.; Pueo, B. Acoustic equations in the presence of rigid porous materials adapted to the finite-difference time-domain method. *J. Comput. Acoust.* **2007**, *15*, 255–269. [[CrossRef](#)]
15. Wilson, D.K.; Collier, S.L.; Ostashev, V.E.; Aldridge, D.F.; Symons, N.P.; Marlin, D.H. Time-domain modeling of the acoustic impedance of porous surfaces. *Acta Acust. United Acust.* **2006**, *92*, 965–975.
16. Wilson, D.K. Simple, relaxational models for the acoustical properties of porous media. *Appl. Acoust.* **1997**, *50*, 171–188. [[CrossRef](#)]
17. Van Renterghem, T.; Botteldooren, D. Numerical evaluation of sound propagating over green roofs. *J. Sound Vib.* **2008**, *317*, 781–799. [[CrossRef](#)]
18. Ferreira, N.; Hopkins, C. Using finite-difference time-domain methods with a Rayleigh approach to model low-frequency sound fields in small spaces subdivided by porous materials. *Acoust. Sci. Technol.* **2013**, *34*, 332–341. [[CrossRef](#)]
19. Suzuki, H.; Omoto, A.; Fujiwara, K. Treatment of boundary conditions by finite difference time domain method. *Acoust. Sci. Technol.* **2007**, *28*, 16–26. [[CrossRef](#)]
20. Zhao, J.; Chen, Z.; Bao, M.; Sakamoto, S. Prediction of sound absorption coefficients of acoustic wedges using finite-difference time-domain analysis. *Appl. Acoust.* **2019**, *155*, 428–441. [[CrossRef](#)]

21. Alomar, A.; Dragna, D.; Galland, M.-A. Time-domain simulation of a flow duct with extended-reacting acoustic liners. *Eforum Acusticum* **2020**, 407–409.
22. Dragonetti, R.; Ianniello, C.; Romano, R. The use of an optimization tool to search non-acoustic parameters of porous materials. In Proceedings of the 33rd International Congress and Exposition on Noise Control Engineering, Prague, Czech Republic, 22–25 August 2004; pp. 3171–3177.
23. Hamet, J.-F.; Berengier, M. Acoustical Characteristics of Porous Pavements: A New Phenomenological Model. In Proceedings of the 1993 International Congress on Noise Control Engineering—Internoise 93—People versus Noise, Leuven, Belgium, 24–26 August 1993.
24. Leclaire, P.; Dupont, T.; Sicot, O.; Gong, X.-L. Propriétés acoustiques des matériaux poreux saturés d’air et théorie de Biot. *J. D’acoustique* **1990**, 3, 29–38.
25. Dragonetti, R.; Ianniello, C.; Romano, R.A. The evaluation of intrinsic non-acoustic parameters of polyester fibrous materials by an optimization procedure. In Proceedings of the 6th European Conference on Noise Control, Tampere, Finland, 30 May–1 June 2006.
26. Moufid, I.; Matignon, D.; Roncen, R.; Piot, E. Energy analysis and discretization of the time-domain equivalent fluid model for wave propagation in rigid porous media. *J. Comput. Phys.* **2022**, 451, 110888. [[CrossRef](#)]
27. Wang, H.; Hornikx, M. Extended reacting boundary modeling of porous materials with thin coverings for time-domain room acoustic simulations. *J. Sound Vib.* **2023**, 548, 117550. [[CrossRef](#)]
28. *ISO 10534-2:1998*; Acoustics—Determination of Sound Absorption Coefficient and Impedance in Impedance Tubes—Part 2: Transfer-Function Method. International Organization for Standardization: Geneva, Switzerland, 1998.
29. Kuttruff, H. *Acoustics: An Introduction*; CRC Press: Boca Raton, FL, USA, 2007.
30. Kane, Y.E.E. Numerical solution of initial boundary value problems involving Maxwell’s equations in isotropic media. *IEEE Trans. Antennas Propag.* **1966**, 14, 302–307. [[CrossRef](#)]
31. Taflove, A.; Hagness, S.C. *Computational Electrodynamics: The Finite-Difference Time-Domain Method*, 3rd ed.; Artech House Publishers: Norwood, MA, USA, 2005.
32. Schneider, J.B. *Understanding the Finite-Difference Time-Domain Method*; School of Electrical Engineering and Computer Science Washington State University: Pullman, DC, USA, 2010; Volume 28.
33. *ISO 10534-1:1996*; Acoustics—Determination of Sound Absorption Coefficient and Impedance in Impedance Tubes—Part 1: Method Using Standing Wave Ratio. International Organization for Standardization: Geneva, Switzerland, 1996.
34. Kuttruff, H. *Room Acoustics*, 5th ed.; Spon Press: London, UK, 2009.
35. Cox, T.J.; D’antonio, P. *Acoustic Absorbers and Diffusers: Theory, Design and Application*; CRC Press: Boca Raton, FL, USA, 2009.
36. *ISO 354:2003*; Acoustics—Measurement of Sound Absorption in a Reverberation Room. International Organization for Standardization: Geneva, Switzerland, 2003.
37. Pereira, M.; Mareze, P.; Godinho, L.; Amado-Mendes, P.; Ramis, J. Proposal of numerical models to predict the diffuse field sound absorption of finite sized porous materials—BEM and FEM approaches. *Appl. Acoust.* **2021**, 180, 108092. [[CrossRef](#)]
38. Tormos, R.; Fernández, A.; Ramis-Soriano, J.; Rico, S.; Vicente, J. Nuevos materiales absorbentes acústicos obtenidos a partir de restos de botellas de plástico. *Mater. Construcción* **2011**, 61, 547–558.

Disclaimer/Publisher’s Note: The statements, opinions and data contained in all publications are solely those of the individual author(s) and contributor(s) and not of MDPI and/or the editor(s). MDPI and/or the editor(s) disclaim responsibility for any injury to people or property resulting from any ideas, methods, instructions or products referred to in the content.